Ultrasonics 53 (2013) 150–156

Contents lists available at SciVerse ScienceDirect

Ultrasonics

journal homepage: www.elsevier.com/locate/ultras

Detecting broken-wire flaws at multiple locations in the same wire of prestressing strands using guided waves

Jiang Xu *, Xinjun Wu, Pengfei Sun

School of Mechanical Science and Engineering, Huazhong University of Science and Technology, Wuhan 430074, PR China

ARTICLE INFO

Article history:
Received 9 February 2012
Received in revised form 23 April 2012
Accepted 3 May 2012
Available online 17 May 2012

Keywords:
Multiple flaws
Broken wire
Recovery length
Prestressing strand
Guided wave

ABSTRACT

Broken wires often occur at multiple locations in the same wire of a strand due to the recovery length, which is defined as the length of the wire taking up its full share of the axial load from the break point. The detection of broken-wire flaws at multiple locations along the same wire is investigated using guided waves below 400 kHz. Herein, a sample with three broken-wire flaws in the same wire is analyzed using magnetostrictive guided waves. Our data show that three flaws are found using the low-frequency guided waves (50 kHz) but only one flaw is found using the high-frequency guided waves (320 kHz). By analyzing the reflection and transmission coefficients at the three different flaws, we observe that the energy exchange decreases as the frequency increases along the same propagating distance. Hence, the recovery length for elastic waves, the length of the wire taking up its full share of elastic-wave energy from the break point, is observed. The recovery length for elastic waves in prestressing strands increases with the frequency. To detect prestressing strands using magnetostrictive guided waves, several one-broken-wire flaws at different locations can be distinguished from in different wires or the same wire by employing both low-frequency waves and high-frequency waves. Nevertheless, we cannot identify in which wire the flaws are located because the magnetostrictive sensor analyzes the whole strand.

1. Introduction

Prestressing strands are widely used in prestressed structures, such as power stations, offshore facilities, and bridges. Strands are exposed to a variety of harmful effects, such as fatigue loading and acidic environments [1,2]. As a result, broken-wire flaws often occur in the individual component wire. The broken-wire flaw not only reduces the strand strength, but it also decreases the load-carrying capacity of prestressed structures, possibly leading to collapse. To guarantee the safety of prestressed structures, many nondestructive testing (NDT) methods, such as visual inspection, magnetic flux leakage testing, and radiographic testing method, are employed to detect prestressing strands [3–5]. However, it is difficult to detect a prestressing strand because it is often embedded or covered with a protective layer.

In recent years, guided wave testing technology has gained attention for NDT and structure health monitoring to prestressing strands [6–17]. Guided waves propagate along the axis of a strand for long distances after launch from a single position. The waves are reflected where damages occur, such as notches or breaks. Thus, using guided waves, strands can be detected quickly. There are various ways to generate guided waves in strands, such as the piezoelectric effect, the thermoelasticity effect, the Lorentz force and the magnetostrictive effect [6–10]. Piezoelectric transducers [9,17] and magnetostrictive sensors [6,8,15] are mostly employed. Beard et al. [9] researched the mode shapes based on the dispersion curves of the grouted tendons and bolts. The low-leakage modes, which the relative amount of in-plane stress to shear stress increased and the amount of mode conversion is reduced, were employed. Rizzo and Di-Scalea [10] characterized the dispersive and attenuating behavior of the L(0,1) and F(1,1) modes in the central straight wire and the peripheral helical wire. They concluded that the surface displacements were responsible for the acoustic coupling. An enhance method of monitoring multi-wire strands is proposed [11]. The largest sensitivity to notch depth is the linear dependence on notch depth in logarithmic scale. A method based on outlier analysis and the wavelet transform for structural damage detection based on guided ultrasonic waves were provided [12]. The general framework is applied to the detection of notch-like defects in a seven-wire strand by using built-in magnetostrictive devices. At numerically investigating the propagation of elastic waves in free helical waveguides, Treyssede [18] proposed a numerical procedure based on a periodic FE approach combined with a specific helical mapping in order to reduce the periodic cell length. Then Treyssede [19] developed a semi-analytical finite element (SAFE) method extended to helical waveguides. Recently, a numerical method was given based on a SAFE

* Corresponding author. Tel./fax: +86 27 87559332.
E-mail address: jiangxu@mail.hust.edu.cn (J. Xu).

0041-624X/$ - see front matter © 2012 Elsevier B.V. All rights reserved.
http://dx.doi.org/10.1016/j.ultras.2012.05.003

technique that relies on a specific non-orthogonal curvilinear coordinate system [14]. A dispersion analysis for a seven wire strand with simplified contact conditions was then performed. The missing notch-frequency phenomenon in the strand was explained using the FE model.

Only a single notch with varying depths in a strand has been detected using guided waves [11,13,15]. Kwun employed a magnetostrictive sensor to inspect the strands with one broken-wire flaw [6,20,21]. The detection of several broken wires in one location was reported in our previous work [22]. Two notches on both sides of the sensors were detected in Rizzo's work [23]. Because bi-directional waves were generated in the strand, the echoes of two notches were not interference. The strand with one broken-wire flaw and a notch on the same side as the sensors was detected using magnetostrictive technology by Di-Scalea et al. [1]. Mijarez employed piezoelectric transducers to detect one notch in a seven-wire aluminum conductor steel reinforced cable [16]. Most investigations have focused on detecting a single flaw or multiple flaws in different wires.

If a wire is broken at one location, then typically, more break points will not occur along the same wire because the stress has been released. Nevertheless, this view does not apply to strands or wire ropes. The contact and friction force among the flawed wire and unbroken neighbor wires can transfer the axial load to the flawed wire. Thus, the flawed wire can regain its share of the load away from the break point. The length of the wire taking up its full share of the axial load is defined as the recovery length (e.g., development length) [24–26]. Therefore, broken-wire flaws often occur at multiple locations along the same wire of a strand [27]. If a single wire is broken in one location, total reflection will occur in the cross-section. Only the first broken-wire flaw can be detected. We therefore ask: can the guided wave method be used to detect broken-wire flaws at multiple locations along the same wire of prestressing strands?

Several studies have investigated the wave propagation along multi-wire cables. Haag et al. [28] studied the wave energy distribution between two rods through friction contact. They concluded that the subsurface wires could be detected through the spread of elastic energy from the surface wires to the subsurface wires. Although the influence of the frequency was not analyzed thoroughly, it was noted that the elastic energy became concentrated near the surface at high frequencies. Baltazar et al. [17] found that the contact force between wires controlled the mode conversion phenomenon between the longitudinal modes and the flexural modes at high frequencies (i.e., above 500 kHz). The decrease of mechanical contact forces between wires prevents energy exchange. Baltazar mentioned that larger radial displacements caused greater energy transfer. The radial displacements at the surface are small at low frequencies but increases as the frequency gets higher. However, the amplitude increases at low frequencies (below 500 kHz). Moreover, the guided waves used to detect strands were usually less than 400 kHz. There is little information available in literature about detecting broken wires at multiple locations along the same wire of prestressing strands using guided waves.

The objective of this work is to explore the detection of broken-wire flaws at multiple locations in the same wire of prestressing strands using guided waves below 400 kHz. Three broken-wire flaws in the same wire are detected using low frequency (50 kHz) guided waves, and only one broken-wire flaw is detected using high frequency (320 kHz) guided waves. The recovery length of elastic waves, the length of the wire taking up its full share of elastic-wave energy from the break point, is observed. The recovery length of elastic waves increases as the frequency of the guided wave increases. Because the elastic energy exchange among wires with a high frequency guided wave is less than this having a low frequency guided wave along the same propagating distance. A method to determine whether two one-broken-wire flaws at different locations are in the same wire or different wires is discussed herein.

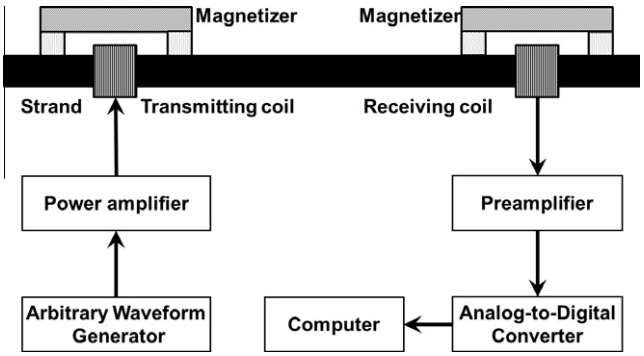

Fig. 2. Schematic of the magnetostrictive guided wave inspection system.

2. Experimental procedure

A prestressing strand sample was composed of seven steel wires where a center wire was enclosed tightly by six helical wires. The specification of the prestressing strand was 15.24 mm diameter, $1*7$-wire steel prestressing strand (ASTM A416-90a, ISO 6934-4). The diameters of the straight wire and the individual helical wires were 5.08 mm. The length of the strand was 5000 mm. There were three broken-wire flaws along the same wire as shown in Fig. 1. The flaws were cut by a grinder and the three flaws were completely through one wire. The width of the three flaws was about 3 mm.

Piezoelectric transducers need to contact the surface of the strands to generate and receive guided waves, but magnetostrictive sensors can generate and receive guided waves without contacting the strands. Therefore, we employed the magnetostrictive technology to detect strands in this experiment. A magnetostrictive guided wave inspection system was employed as shown in Fig. 2. The transmitter consisted of a transmitting coil and a magnetizer. The coil had 60 turns of American wire gauge 26 enameled wire and 17 mm in diameter. The structure of the coil, which was similar as Rizzo's coil [1], is shown in Fig. 3. The center distance of the three-part coil was adjustable to satisfy the response requirements for different frequencies. The magnetizer was made of permanent magnets with an armature and provided a static axial bias magnetic field to cancel the second-harmonic generation

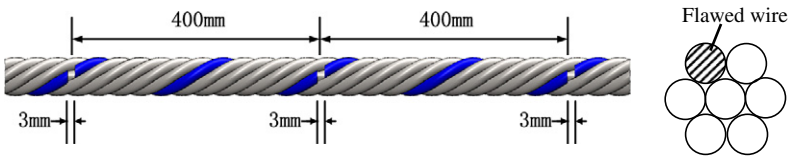

Fig. 1. The distribution of three broken-wire flaws in the prestressing strand.

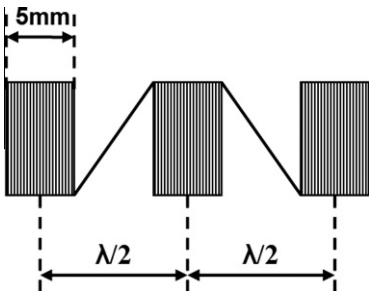

Fig. 3. Structure of the transmitting coil and the receiving coil. The wavelength is λ.

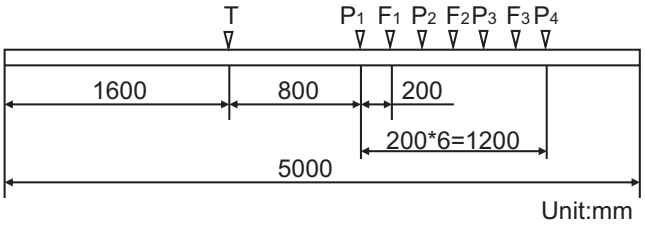

Fig. 4. Experimental arrangement for detecting flaws. T is the location of the transmitter. P1, P2, P3, and P4 are the locations where the receiver was placed. F1, F2, and F3 are the broken-wire flaws.

and improve the coupling efficiency. The transmitter generated longitudinal mode elastic waves in strands using the Joule effect. The receiver consisted of a receiving coil and magnetizers. The receiving coil had 150 turns of American wire gauge 36 enameled wire and 17 mm in diameter. The structure of the receiving coil was similar to the transmitting coil. The receiving coil induced the wave based on the Villari effect. The exciting coil was excited by applying three cycles sinusoidal tone burst with 120 V peak-to-peak amplitude using a signal generator and a power amplifier. The voltage induced in the receiving coil was amplified (approximately 66 dB). The signals were subsequently digitized using an A/D card, which works at 2MS/s. To reduce white noise, the repeated times of each experiment was 300. The signals were stored in a personal computer.

The experiment consisted of two stages.

First, attenuation coefficients were obtained from the strand before making the flaws. The transmitter was fixed; the receiver was placed at three different distances (1200 mm, 1600 mm, and 2000 mm) from the transmitter. It is well-known that magnetostrictive transduction phenomenon works efficiently at low-frequencies. However, in Rizzo's study, the operating frequency approached 400 kHz. A frequency of 320 kHz was chosen as the low attenuation value [10]. Therefore, a magnetostrictive sensor (resonant over frequencies from 50 to 400 kHz with a 10 kHz step), was employed to generate and detect guided waves in the strand. The wave mode was the first longitudinal mode (L(0,1)). Only the symmetrical modes were received because the sensor was axisymmetric.

Second, a sample with three broken-wire flaws in the same wire was analyzed using guided waves. The flaws were labeled as F1, F2 and F3 as shown in Fig. 4. The transmitter was fixed at position T and the receiver was placed at P1, P2, P3, and P4, respectively. Guided waves from 50 to 400 kHz with a 10 kHz step were generated along the strand.

3. Results and discussions

3.1. Attenuation coefficients of waves in the strand prior to creating broken-wire flaws

One group of data, with an excitation frequency was 50 kHz, is given in Fig. 5. The data were acquired before broken-wire flaws were introduced at three different distances between the transmitter and the receiver. The peak–peak value of the signals was employed to evaluate the measurements in the following analysis.

The first passing signal (FPS) was used to calculate the attenuation coefficient of the wave in the strand. The relationship between the attenuation coefficient and the excitation frequency is shown in Fig. 6. The valley at 100 kHz was the "notch frequencies" as mentioned in Kwun et al. [29], Rizzo and Di-Scalea [10] and Laguerre and Treyssede's [14] papers. The notch frequencies would change with the tensile load to the strand. The highest losses (about 6.5 dB/m) was found at 100 kHz for L(0,1) in the experiment. The notch frequencies should be avoided for detect the prestressing strand. The result was similar to Rizzo's [10]. In next section, the incident waves and the reflected waves were compensated with the attenuation coefficients to calculate the reflection coefficients and the transmission coefficients.

3.2. Flaw detection over frequencies from 50 to 400 kHz using guided waves

We explored the feasibility of detecting broken-wire flaws at multiple locations along the same wire of prestressing strands using guided waves. Data obtained at 50 kHz (low frequency)

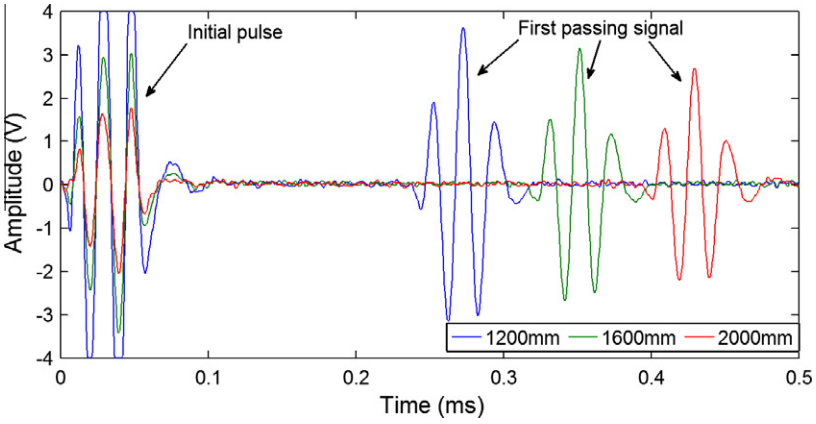

Fig. 5. Data taken from a strand without defects at three different distances (1200 mm, 1600 mm and 2000 mm) between the transmitter and the receiver. The excitation frequency was 50 kHz.

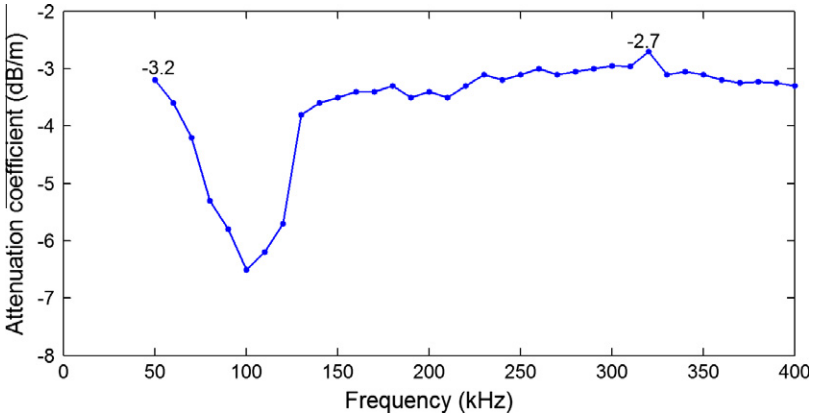

Fig. 6. The relationship between the attenuation coefficient and the excitation frequency.

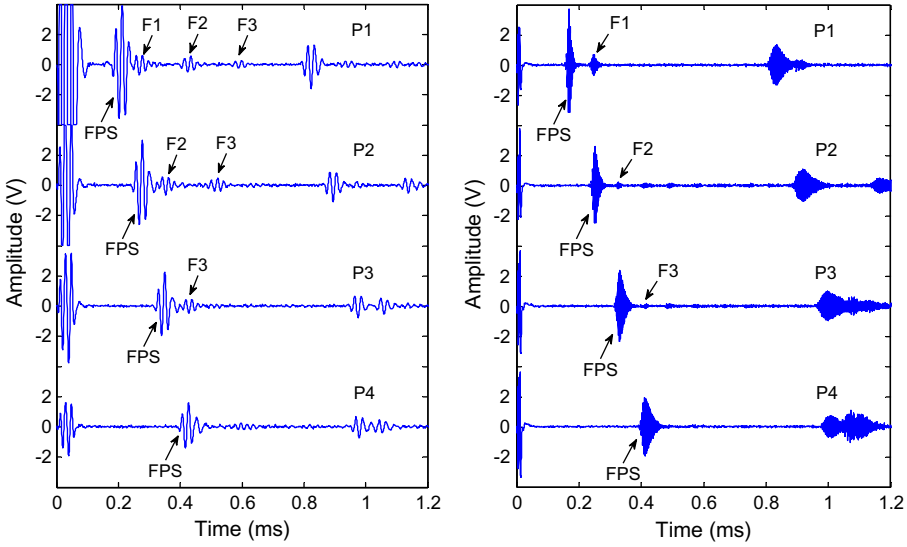

(a) The excitation frequency was 50 kHz (b) The excitation frequency was 320 kHz

Fig. 7. Data obtained from the sample with three broken-wire flaws along the same wire using guided waves.

and 320 kHz (high frequency) are shown in Fig. 7. As shown in Fig. 7a, three broken-wire echoes were obtained at 50 kHz when the receiver was placed at P1. By comparison, only the F1 echo was obtained at 320 kHz when the receiver was placed at P1. The results indicate that the multiple-location broken-wire flaws along the same wire could be detected with low-frequency waves but not with high frequency waves. In next section, we explored the phenomena further using the reflection and transmission coefficients at the three broken-wire flaws.

To analyze the wave reflection and transmission at the flaws, the reflection and transmission coefficients are denoted as shown in Fig. 8. The wavelength of the waves was greater than the width of the broken-wire flaws, so reflections from the back edge of the broken-wire flaws were ignored. Greater contributions from α_2 and α_3 led to a larger energy transfer from the unbroken neighboring wires to the flawed wire. Greater contributions from β_2 and β_3 led to less energy reflection from the flaws. Greater contributions from β_{21}, β_{32} and β_{31} led to a larger energy transfer from the flawed wire to the unbroken neighbor wires.

If wave attenuation in the strand was taken into account, the attenuation coefficient and the propagated distance were necessary to compensate the signals. The compensated signals were used to compute the reflection and transmission coefficients. The details for computing the reflection and the transmission coefficients were given here, where the compensated flaw echo and the incident wave were used to compute the reflection coefficients. The reflection coefficients were calculated as written below [30]:

$$\alpha_{i-f} = \frac{V_{pp-echo}}{10^{\gamma_f L/20}} \cdot \frac{1}{V_{pp-FPS}} \quad (1)$$

where f is the frequency of wave; $V_{pp\text{-}echo}$, the Vpp of the ith flaw echo; γ_f, the attenuation coefficient of wave at f; L, the propagated distance of the echo; $V_{pp\text{-}FPS}$ is the V_{pp} of FPS.

For example, the V_{pp} of FPS was 7.25 V and the V_{pp} of F1 echo was 1.34 V when the receiver was placed at P1 of the sample with a 50 kHz excitation frequency. Considering the additional propagated distance of F1 echo (400 mm), the V_{pp} of F1 echo after compensating was approximately 1.55 V. Therefore, it was determined that $\alpha_{1-50kHz}$ was approximately 21.4%.

The incident wave and the transmission wave of the flaws were used to compute the transmission coefficients. The compensated method was similar to Eq. (1). For example, the V_{pp} of FPS was 7.25 V at P1 and 5.56 V at P2 at 50 kHz. Considering the additional propagated distance, which was 400 mm, the V_{pp} of FPS at P2 was approximately 6.45 V after compensating. Therefore, $\beta_{1-50kHz}$ was 89.0%.

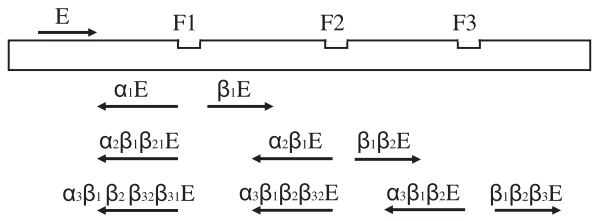

E: the amplitude of the incident wave

i: the serial number of flaws

α_i: reflection coefficients at the *ith* flaw

β_i: the transmission coefficients of the wave passing the *ith* flaw

j: the reflected wave toward the serial number of flaws

β_{ij}: the transmission coefficients of the *ith* flaw echo to the *jth* flaw

Fig. 8. Schematic diagrams of the reflection and transmission coefficients at the three flaws.

By a similar approach, we obtained all of the reflection and transmission coefficients of the sample from 50 kHz to 400 kHz. Fig. 9 shows the reflection and transmission coefficients at three flaws as a function of the different excitation frequencies applied to the strand.

From Fig. 9a, the reflection coefficient and the transmission coefficient at F1 were almost the same from 50 kHz to 400 kHz. The reflection coefficients α_2 and α_3 gradually decreased with the increase in frequency and the transmission coefficients β_2 and β_3 gradually increased with an increase in frequency as shown in Fig. 9b and c. These results indicated that the elastic energy being transmitted from unbroken neighbor wires to the flawed wire decreased with the frequency increase along the same propagating distance. Here, the recovery length of elastic waves (like the recovery length of stress) was defined as "the length of the wire taking up its full share of elastic-wave energy from the break point". We also determined that the recovery length of elastic waves from 50 kHz to 80 kHz was less than 200 mm. The transmission coefficients of the flaw echoes, β_{21}, β_{32} and β_{31}, decreased with an increase in frequency from Fig. 9d. These results indicated that the elastic energy transmitted from the flawed wire to the unbroken neighbor wires decreased with an increase in frequency.

The following analysis mainly focused on the incident wave and the reflection wave of F2 propagating in the strand. The coefficients of interest were α_1, α_2, β_1, β_2 and β_{21}. We divided the processing into eleven stages. Fig. 10a shows the stages of wave propagation at 50 kHz. The section of the flawed wire before F1 was denoted as S1. The section of the flawed wire between F1 and F2 was denoted as S2.

Stage I: Before the wave arrived at the F1 position, the energy in six peripheral helical wires, which was greater than in the center straight wire, was almost the same [10].
Stage II: After the wave passes through F1, the wave energy in the start position of S2 was approximately equal to zero because total reflection occurs at the end position of S1.
Stage III: The energy in the center straight wire and the peripheral helical wires near the flawed wire leaked to the flawed wire when the wave propagated from F1 to F2 [25,26,31,32].
Stage IV: When the propagation distance increased, energy exchange occurred among the wires.
Stage V: The wave energy in the flawed wire recovered, which was the same as other peripheral helical wires.
Stages VI and VII: When the wave arrived at F2, the energy in the flawed wire was reflected and the wave in other wires passed through. As $\alpha_{1-50kHz}$ was approximately equal to $\alpha_{2-50kHz}$ and $\beta_{1-50kHz}$ was approximately equal to $\beta_{2-50kHz}$, recovery of the wave energy in the flawed wire was confirmed.

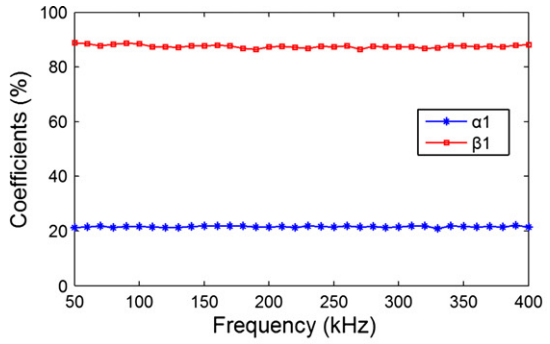

(a) Reflection coefficients and transmission coefficients at F1 as a function of different excitation frequencies

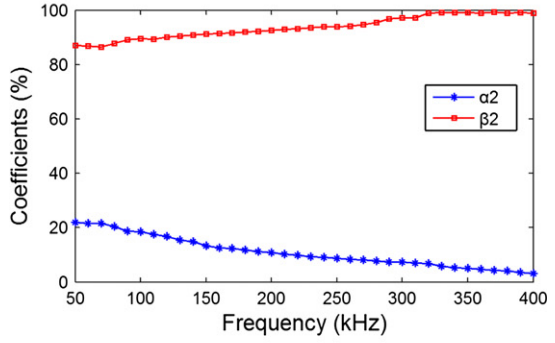

(b) Reflection coefficients and transmission coefficients at F2 as a function of different excitation frequencies

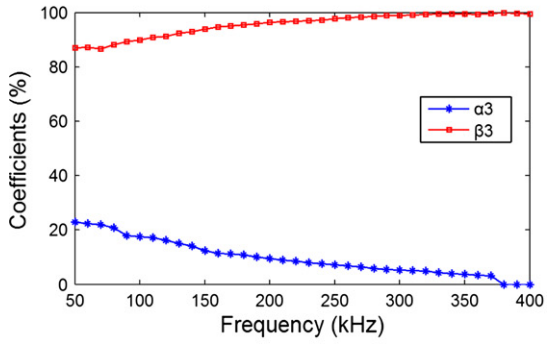

(c) Reflection coefficients and transmission coefficients at F3 as a function of different excitation frequencies

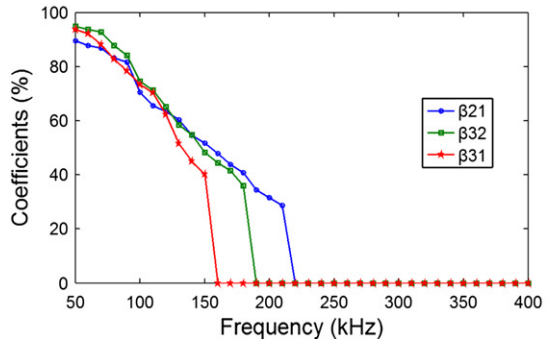

(d) Transmission coefficients of the flaw echoes passing the flaws as a function of different excitation frequencies (Zero means the amplitude of the signal is too small to identify.)

Fig. 9. Reflection coefficients and transmission coefficients of guided waves at three broken-wire flaws.

Stages VIII–X: Similarly, the echo of F2 propagating from F2 to F1 might leak to other wires. Based on the value of $\beta_{21-50kHz}$

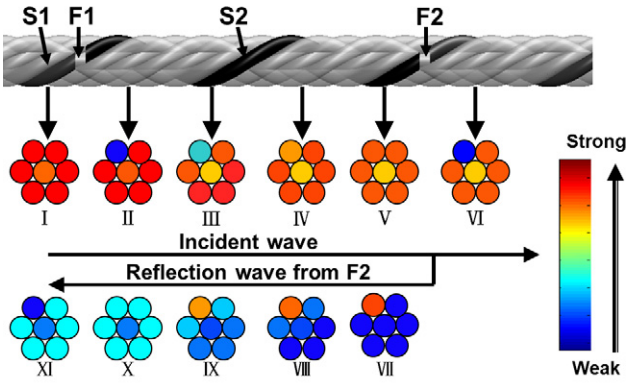

(a) The excitation frequency was 50 kHz.

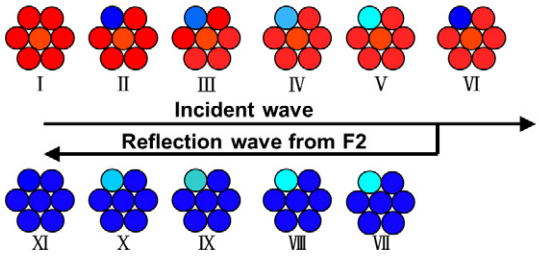

(b) The excitation frequency was 320 kHz

Fig. 10. Schematic diagrams of energy assignments in the strand with three broken-wire flaws along the same wire.

(89.5%), which was approximately equal to $\beta_{1-50kHz}$ (89.0%), the energy in other peripheral helical wires and the center straight wire recovered.

Stage XI: When the echo of F2 arrived at F1, the wave in the flawed wire was reflected by F1 and the wave in other wires passes through.

Therefore, an echo of F2 was obtained at 50 kHz when the receiver was placed at P1. Based on the same principle, an echo of F3 was obtained at 50 kHz when the receiver was placed at P1. Here, $\beta_{32-50kHz}$ or $\beta_{31-50kHz}$ was greater than $\beta_{21-50kHz}$, because multiple reflections from F2 among the flaws were superimposed on the echo of F3. The above results indicated that the recovery length for a 50 kHz wave was shorter than 200 mm.

However, wire breaks at three locations along the same wire could not be detected under the same conditions using a 320 kHz wave. Only F1 was detected when the receiver was placed at P1, as shown in Fig. 5b. Compared to the data obtained using a 50 kHz wave, $\alpha_{2-320kHz}$ (6.8%) and $\beta_{2-320kHz}$ (98.0%) indicated that there was less energy leaking to the flawed wire from the other wires over stages III–V and less energy leaking to other wires from the flawed wire at stages VIII–X as shown in Fig. 10b. Therefore, the echo of F2 was not obtained when the receiver was placed at P1. This result indicates that the recovery length for the 320 kHz wave was longer than 200 mm. In other words, the recovery length of the elastic waves in the strand became longer as the frequency increased.

From the reflection and transmission coefficients at three broken-wire flaws at different frequencies, we determined that the elastic energy exchange among wires increased at lower frequencies and was markedly reduced at high frequencies. These results were similar to Kwun's experimental observations using pipes [33]. Kwun's results showed that the discontinuity signals from the mechanical clamps were greatly reduced at high frequencies. Mechanical clamps were not beneficial to the guided wave testing of the pipe. Hence, they suggested that the high frequency guided wave could be more appropriately utilized to detect pipes with mechanical attachments. In contrast, we suggested that a low frequency guided wave was better to detect multiple-location broken-wire flaws in the same wires.

Our research also provided a method to determine whether two broken-wire flaws were in the same wire or different wires by employing both low frequency waves and high frequency guided waves. When two broken-wire flaws were in the strand, guided waves were employed to detect the strand. If the two flaw echoes were obtained using both low frequency waves and high frequency waves, we could deduce that the two broken-wire flaws were in different wires. If the two flaw echoes were obtained using low frequency waves and only one flaw echo was obtained using high frequency waves, we deduced that the two broken-wire flaws were in the same wire. Nevertheless, we could not identify which wire the flaws were located in as the magnetostrictive sensor analyzed the whole strand.

When the method is brought to the field, the strengths of the method are:

(1) If we only employ the high frequency waves to detect the prestressing strand, the broken-wire flaws in the same wire will be missed. The problem can be avoided using this method.
(2) Using this method, we can determine whether multiple one-broken-wire flaws at different locations are in the same wire or different wires. The result will provide more information to maintenance and repair the prestressed structures.

The weaknesses of the method are:

(1) When the prestressing strand is coated by concrete in the field, the losses of waves in the strand will increase greatly. This method is difficult to be applied to detect the strand.
(2) If multiple one-broken-wire flaws at different locations in the same wire are detected, we could not identify which wire the flaws are located in.

4. Conclusions and future work

The detection of broken-wire flaws at multiple locations in the same wire of prestressing strands using guided waves is investigated. Three broken-wire flaws along the same wire are detected using low frequency guided waves. Only the first broken-wire flaw is detected using high frequency guided waves. Energy exchange among the wires decreases along the same propagating distance as the frequency increases. In other words, the recovery length of elastic waves in prestressing strands increases with an increase in frequency. This study provides a method to determine whether two one-broken-wire flaws at different locations are in the same wire or different wires by employing both low frequency waves and high frequency waves.

The multiple location broken-wire flaws in the same wire of the loaded strand will be studied in future work. In addition, the relationship among the frequency, the loaded stress and the recovery length of elastic waves will be investigated.

Acknowledgments

This research was supported by the National Key Technology R&D Program of China (Grant No. 2011BAK06B05), the Special Fund for Basic Scientific Research of Central Colleges (Grant No. 2011QN130) and the Natural Science Foundation of Hubei Province of China (Grant No. 2011CDB286). The author (J. Xu) appreciates Allen and Carolyn Green's suggestions.

References

[1] F.L. Di-Scalea, P. Rizzo, F. Seible, Stress measurement and defect detection in steel strands by guided stress waves, Journal of Materials in Civil Engineering 15 (3) (2003) 219–227.

[2] S. Austin, R. Lyons, M. Ing, Electrochemical behavior of steel-reinforce concrete during accelerated corrosion testing, Corrosion 60 (2) (2004) 203–212.

[3] M.E. Elliott, E. Heymsfield, Inspection of Luling bridge cable stays: case study, Journal of Construction Engineering and Management 129 (2) (2003) 226–230.

[4] A.B. Mehrabi, In-service evaluation of cable-stayed bridges, overview of available methods and findings, Journal of Bridge Engineering 11 (6) (2006) 716–724.

[5] X.J. Wu, Y.H. Kang, H.G. Chen, Nondestructive testing method and technique for cable-stayed bridge steel cables, Key Engineering Materials 270–273 (7) (2004) 1493–1499.

[6] H. Kwun, C.M. Teller, Detection of fractured wires in steel cables using magnetorestrictive sensors, Materials Evaluation 52 (4) (1994) 503–507.

[7] T. Yamasaki, S. Tamai, M. Hirao, Optimum excitation signal for long-range inspection of steel wires by longitudinal waves, NDT & E International 34 (3) (2001) 207–212.

[8] L. Laguerre, J.C. Aime, M. Brissaud, Magnetostrictive pulse-echo device for non-destructive evaluation of cylindrical steel materials using longitudinal guided waves, Ultrasonics 39 (7) (2002) 503–514.

[9] M.D. Beard, M.J.S. Lowe, P. Cawley, Ultrasonic guided waves for inspection of grouted tendons and bolts, Journal of Materials in Civil Engineering 15 (3) (2003) 212–218.

[10] P. Rizzo, F.L. Di-Scalea, Wave propagation in multiwire strands by wavelet-based laser ultrasound, Experimental Mechanics 44 (4) (2004) 407–415.

[11] P. Rizzo, F.L. Di-Scalea, Feature extraction for defect detection in strands by guided ultrasonic waves, Structural Health Monitoring 5 (3) (2006) 297–308.

[12] P. Rizzo, Ultrasonic wave propagation in progressively loaded multiwire strands, Experimental Mechanics 46 (3) (2006) 297–306.

[13] P. Rizzo, E. Sorrivi, F.L. Di-Scalea, E. Viola, Wavelet-based outlier analysis for guided wave structural monitoring: application to multi-wire strands, Journal of Sound and Vibration 307 (1–2) (2007) 52–68.

[14] L. Laguerre, F. Treyssede, Investigation of elastic modes propagating in multi-wire helical waveguides, Journal of Sound and Vibration 329 (10) (2010) 1702–1716.

[15] Z.H. Liu, J. Zhao, B. Wu, Y. Zhang, C.F. He, Configuration optimization of magnetostrictive transducers for longitudinal guided wave inspection in seven-wire steel strands, NDT&E International 43 (6) (2010) 484–492.

[16] R. Mijarez, F. Martinez, A. Baltazar, Real time damage detection system using guided waves in ACSR cables, In: Proceedings of the Annual Review of progress in Quantitative NDE, 2010, pp. 18–23.

[17] A. Baltazar, C. Hernandez, B. Manzanares-Martinez, Study of wave propagation in a multiwire cable to determine structural damage, NDT&E International 43 (8) (2010) 726–732.

[18] F. Treyssede, Numerical investigation of elastic modes of propagation in helical waveguides, Journal of the Acoustical Society of America 121 (6) (2007) 3398–3408.

[19] F. Treyssede, Elastic waves in helical waveguides, Wave Motion 45 (4) (2008) 457–470.

[20] H. Kwun, J.J. Hanley, K.A. Bartels, Recent developments in nondestructive evaluation of steel strands and cables using magnetostrictive sensors, In: Oceans'96 MTS/IEEE Conference Proceedings, 1996, pp. 144–148.

[21] K.A. Bartels, H. Kwun, J.J. Hanley, Magnetostrictive sensors for the characterization of corrosion in rebars and prestressing strands, In: Proc SPIE 2946, 1996, pp. 40–50.

[22] J. Xu, X.J. Wu, L.Y. Wang, C. Huang, Y.H. Kang, Detecting the flaws in prestressing strands using guided waves based on the magnetostrictive effect, Insight 49 (11) (2007) 647–650.

[23] P. Rizzo, F.L. Di-Scalea, Ultrasonic inspection of multi-wire steel strands with the aid of the wavelet transform, Smart Materials and Structures 14 (4) (2005) 685–695.

[24] M. Raoof, I. Kraincanic, Recovery length in multi-layered spiral strands, Journal of Engineering Mechanics 121 (7) (1995) 795–800.

[25] M. Raoof, I. Kraincanic, Determination of wire recovery length in steel cables and its practical applications, Computers & Structures 68 (5) (1998) 445–459.

[26] A. Gjelsvik, Development length for single wire in suspension bridge cable, Journal of Structural Engineering 117 (4) (1991) 1189–1200.

[27] M. Raoof, Y.P. Huang, Wire recovery length in suspension bridge cable, Journal of Structural Engineering 118 (12) (1992) 3255–3267.

[28] T. Haag, B.M. Beadle, H. Sprenger, L. Gaul, Wave-based defect detection and interwire friction modeling for overhead transmission lines, Archive of Applied Mechanics 79 (2009) 517–528.

[29] H. Kwun, K.A. Bartels, J.J. Hanley, Effect of tensile loading on the properties of elastic wave in a strand, Journal of the Acoustical Society of America 103 (6) (1998) 3370–3375.

[30] J.D.N. Cheeke, Fundamentals and Applications of Ultrasonic Waves, CRC Press, Boca Raton FL, 2002.

[31] S. Machida, A.J. Durelli, Response of a strand to axial and torsional displacements, Journal of Mechanical Engineering Science 15 (4) (1973) 241–251.

[32] B.K. Gnanavel, D. Gopinath, N.S. Parthasarathy, Effect of friction on coupled contact in a twisted wire cable, Journal of Applied Mechanics 77 (2) (2010) 024501-1–024501-6.

[33] H. Kwun, S.Y. Kim, G.M. Light, Improving guided wave testing of pipelines with mechanical attachments, Materials Evaluation 68 (8) (2010) 927–932.